Nanotubes

DOI: 10.1002/ange.200501341

A Template-Based Electrochemical Method for the Synthesis of Multisegmented Metallic Nanotubes**

Woo Lee, Roland Scholz, Kornelius Nielsch, and Ulrich Gösele*

Tubular nanostructures have stimulated extensive research efforts in recent years because of their technological importance in advanced electronic or magnetic devices[1] and prospective applications in catalysis,[2] sensors,[3] and biological separation and transport.[4] To date, various methods[5] including reductive sulfidization,[6] thermal decomposition of precursors,[7] atomic layer deposition (ALD),[8] hydrothermal pyrolysis,[9] galvanic replacement reactions,[10] and surfactant- or template-based growth[11] have been developed for the fabrication of such tubular nanostructures. Among them, template-based synthesis using anodic aluminum oxide (AAO) or track-etched polymer membranes has attracted much attention, because it provides several distinct advantages over other approaches. It offers a convenient way for producing structurally uniform nanostructures periodically aligned in template matrices. A wide range of materials including metals, semiconductors, and polymers have been prepared in the form of nanotubes.[12] However, few examples have been reported on the fabrication of metal nanotubes despite their technological importance. The development of a generalized method for the fabrication of aligned metal-nanotube arrays remains a challenge. Precise control of the nanotube growth process and formation of well-aligned arrays will greatly assist investigations of their physical properties and their potential use in nanoscale fluidics, chemical and biological separations, sensors, and catalysts.

Herein, we report a novel approach for the preparation of metallic nanotubes based on the preferential electrodeposition of a metal along the pore walls of an AAO membrane in the presence of metallic nanoparticles on the wall surfaces (Figure 1). Several reports on the immobilization of metallic nanoparticles on the pore walls of AAO have been published previously. Schmid and co-workers showed that Au nanoparticles can be self-assembled on AAO channels modified with organosilane molecules, which function as molecular anchors binding the nanoparticles.[13] More recently, Rubin-

[*] Dr. W. Lee, Dr. R. Scholz, Dr. K. Nielsch, Prof. Dr. U. Gösele
Max Planck Institute of Microstructure Physics
Weinberg 2, 06120 Halle (Germany)
Fax: (+49) 345-5511-223
E-mail: woolee@mpi-halle.de

[**] Financial support from the German Federal Ministry for Education and Research (BMBF, Project No. 03N8701) is gratefully acknowledged.

Supporting information for this article is available on the WWW under http://www.angewandte.org or from the author.

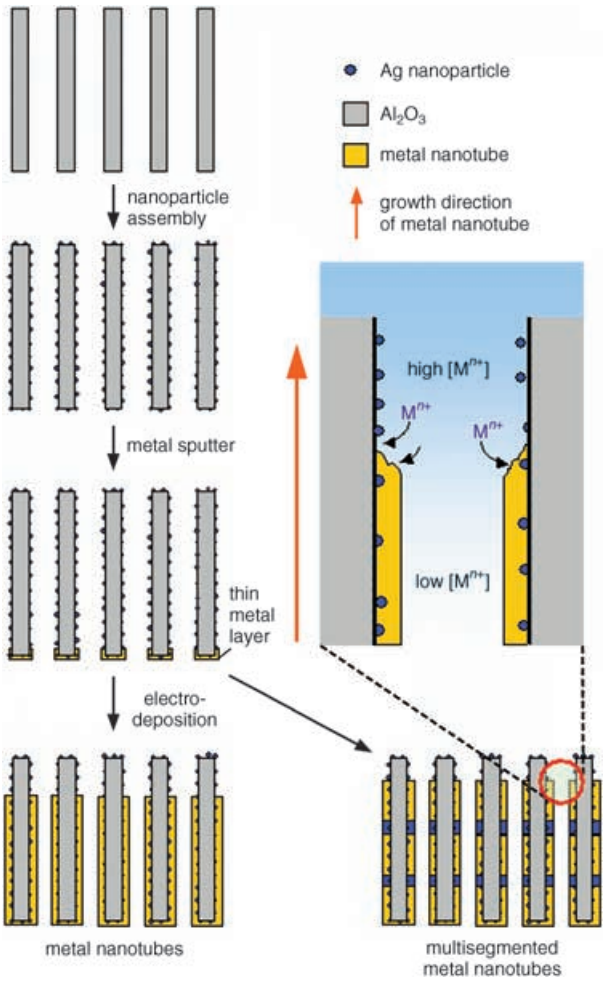

Figure 1. Procedure for the preparation of metal nanotubes and the proposed mechanism of metal nanotube growth (see text).

stein and co-workers demonstrated the preparation of Au nanoparticle nanotubes (NPNTs) by introducing a colloid solution of Au nanoparticles into the pores of an organosilane-modified AAO, followed by spontaneous coalescence of the surface-bound Au nanoparticles.[14] In an alternative approach, Johansson et al. deposited Pd nanoparticles on the pore walls of AAO by using a sequential electroless deposition technique, in which a palladium complex ($[Pd(NH_3)_4]^{2+}$) was thermally reduced to metallic Pd.[15] In the present study, metallic nanoparticles (for example, Ag) were immobilized on the pore walls of an AAO membrane by the spontaneous reduction of Ag^I by Sn^{II}, which is a modification of the previously established sensitization–preactivation process of AAO[16] or polymer membranes[17] prior to the electroless deposition of metals. To induce the selective reduction of metal cations on the surfaces of oxide membranes, Sn^{II} was first deposited on the pore walls by immersing the membranes in an aqueous solution of $SnCl_2$. After a drying step, the resulting membranes were soaked in an aqueous solution of $AgNO_3$. These two steps constitute one deposition cycle and were repeated several times (typically six cycles). The standard reduction potential of Sn^{IV}/Sn^{II} (0.151 V versus standard hydrogen electrode, SHE) is lower than that of the Ag^I/Ag^0 pair (0.80 V versus SHE). Therefore, the surface-bound $Sn^{II}_{surface}$ cations would be spontaneously oxidized into Sn^{IV}, thus producing discrete metallic Ag nanoparticles on the surface of the Sn^{II}-treated AAO membrane upon immersion in an aqueous solution of $AgNO_3$ [Eq. (1)].

$$2\,Ag^{I}_{aq} + Sn^{II}_{surface} \rightarrow 2\,Ag^{0}_{surface} + Sn^{IV}_{surface} \quad (1)$$

This process results in homogeneous deposition of metal nanoparticles over the entire surface (pore walls and faces) of AAO membranes (Figure 2a). The size and the number of

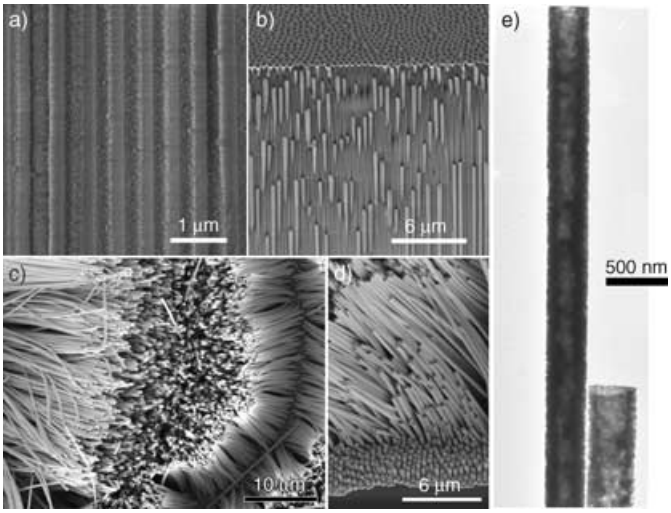

Figure 2. a) Cross-sectional SEM image of the Ag-nanoparticle-immobilized anodic aluminum oxide (AAO) membrane. b) Cross-sectional SEM image of the Au nanotube–AAO composite showing Au nanotubes embedded in the alumina matrix. c) and d) SEM images of Au nanotubes after removal of alumina matrix with NaOH (1.0 M); part d) illustrates the open-end tips of Au nanotubes at the levels of different length. e) Representative TEM image of Au nanotubes showing their tubular structure.

metal nanoparticles depend on the number of deposition cycles. The average particle size determined by TEM analyses was 11 ± 4 nm (Supporting Information). Unlike the Au NPNTs reported by Rubinstein and co-workers[14] which showed good electrical conductivity with a specific resistivity of 6 Ω cm, our Ag-nanoparticle-modified AAO membranes exhibited a typical insulating behavior even after 10 deposition cycles. This finding indicates that the Ag nanoparticles immobilized on the surfaces of AAO membranes are isolated from each other without the formation of a continuous conduction path for current transport. Electrodeposition of Au at current densities ranging from 2.2 to 2.5 mA cm^{-2} resulted in the formation of Au nanotubes embedded in the alumina matrix (Figure 2b). Subsequent removal of the oxide matrix with NaOH (1.0 M) led to the release of Au nanotubes with surfaces decorated with Ag nanoparticles (Figure 2c,d). The presence of Ag nanoparticles on the surface of the metal nanotubes is inevitable, and results in mixed-metal nanotubes. TEM investigations of Au nanotubes revealed that the average outer diameter of the nanotubes is 330 nm (Figure 2e). Further evidence for the tubular nanostructure was

obtained directly from water permeation experiments through the gold nanotube arrays embedded in the alumina matrix: a drop of water placed on one side of the membrane was transported to the other side.

In the process described herein, the growth of metal nanotubes starts at the base-metal electrode at the bottom of the pores (that is, a bottom-up deposition of metal) as a result of the nonconducting nature of the nanochannels. It is believed that Ag nanoparticles immobilized on the oxide nanochannel surfaces play a key role in the growth of the metallic nanotubes, and enable preferential electrodeposition of metal along the nanochannel surfaces. Nanotube formation in this electrodeposition process can be understood in terms of the relative rates of deposition and the diffusion of metal ions. It is believed that the deposition process takes place at the tube tips, and therefore the deposition interfaces and the diffusion layers of metal ions move dynamically with the growth process of the tubes (Figure 1). Once a small conducting path is created by electrodeposition between the tube tip and an isolated Ag nanoparticle, the deposition interface will move toward the recently created area, and a majority of the metal ions will be deposited on the newly connected nanoparticle until another isolated particle is electrically connected. This electrodeposition effect establishes a depletion layer of metal ions, and thus the ion concentration below the tube tips should be very low, and the metal deposition on the inner tube wall should be negligible. Our assumptions were proven by electrodeposition experiments with different deposition rates. The electrodeposition carried out at a low current density ($< 0.4\ mA\,cm^{-2}$), at which the focusing effect at the tube tip could be neglected as a result of the slow deposition rate, produced only arrays of solid metal nanorods. In contrast, the electrodeposition performed at a high current density ($> 3.0\ mA\,cm^{-2}$) resulted in mechanically unstable metal nanotubes with highly porous wall surfaces (Supporting Information).

For cases in which the whole surface of the membrane is electrically conductive, electrodeposition of metal should occur evenly over the entire membrane surface at the same time. In other words, radial growth of metal nanotubes occurs inside the nanochannels, gradually decreasing the channel diameter. The underpotential deposition (UPD) technique is required[18] for the fabrication of pore walls of uniform thickness over the whole length of the membranes. The deposition rate must be sufficiently lower than that of the axial mass transfer of metal cations to guarantee a homogeneous ion concentration over the whole pore length.

By taking advantage of the preferential deposition of metal along the wall surfaces of oxide nanochannels, we were able to prepare multisegmented metallic nanotubes with a bimetallic stacking configuration along the nanotube axes. Figure 3 shows representative SEM images of multisegmented metallic nanotubes with a stacking configuration of Au-Ni-Au-Ni-Au, before (Figure 3a) and after (Figure 3b,c) removal of the alumina matrix with a solution of NaOH (1.0 M). The average outer diameter of the nanotubes was estimated to be 300 nm. Ni segments about 800 nm long with a dark image contrast can be clearly observed between adjacent Au nanotube sections (Figure 3c; see also the color-enhanced view of Au–Ni segments in Figure 3a). This contrast in the SEM images results from differences in the intensity of backscattered electrons from the two metals. In this nanofabrication process, various metallic segments (Ag, Au, Pt, Pd, Fe, Co, Ni, etc.) can be incorporated into the nanotube structure, thus enabling the fabrication of barcode-type nanotubes.[19] The length of each metal segment can be tuned by controlling the amount of total integrated charges involved in the electrochemical reaction. Such a unique capacity for tailoring the nanotube structure could provide an opportunity for engineering the physical properties of nanotube materials.

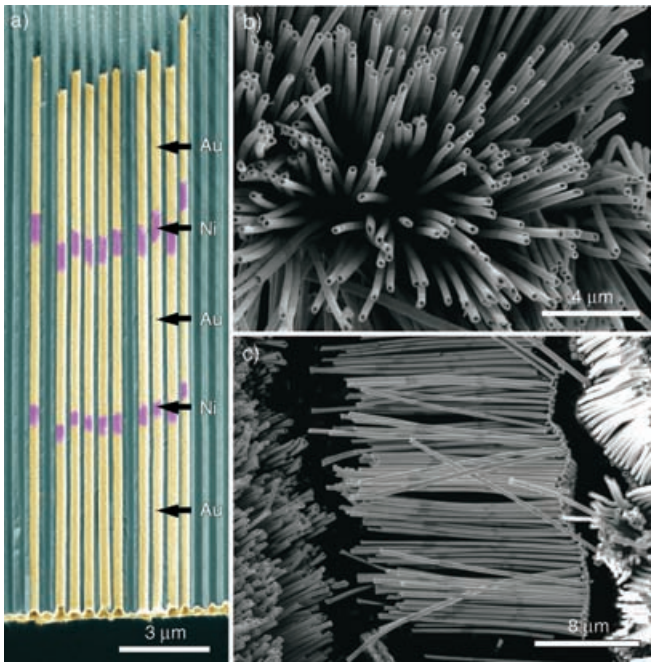

Figure 3. SEM images of multisegmented metal nanotubes with a stacking configuration of Au-Ni-Au-Ni-Au along the nanotube axis. a) Cross-sectional SEM image of as-prepared metal nanotube–AAO composite, which shows metal nanotubes embedded in an alumina matrix. The signals from Au and Ni are shown in yellow and purple, respectively. b) and c) SEM images of multisegmented metal nanotubes after removal of alumina matrix with NaOH (1.0 M); part c) clearly shows the stacking configuration of multisegmented metal nanotubes in which the segments with bright and dark image contrasts correspond to Au and Ni, respectively.

Arrays of continuous Ni nanotubes and of multisegmented nanotubes (Au-Ni-Au-Ni-Au stacking configuration, Figure 3) were examined by a superconducting quantum interference device (SQUID) magnetometer at 298 K for comparison of their magnetic properties. The corresponding hysteresis loops are presented in Figure 4. With the magnetic field applied along the nanotube axis ($\parallel$), both samples showed coercivities $H_{c\parallel}$ in the range of 85 to 90 $A\,m^{-1}$ and relatively low remanence values (4 and 17%). As the saturation field $H_{s\parallel} \gg H_{c\parallel}$, both samples exhibited reversible magnetic behavior. The nanowire diameter was at least one order of magnitude larger than the magnetic exchange length for nickel $\lambda_{Ni} \approx 13$ nm, and we therefore assume that the Ni nanotubes switched by a curling-like switching mode.[20] The

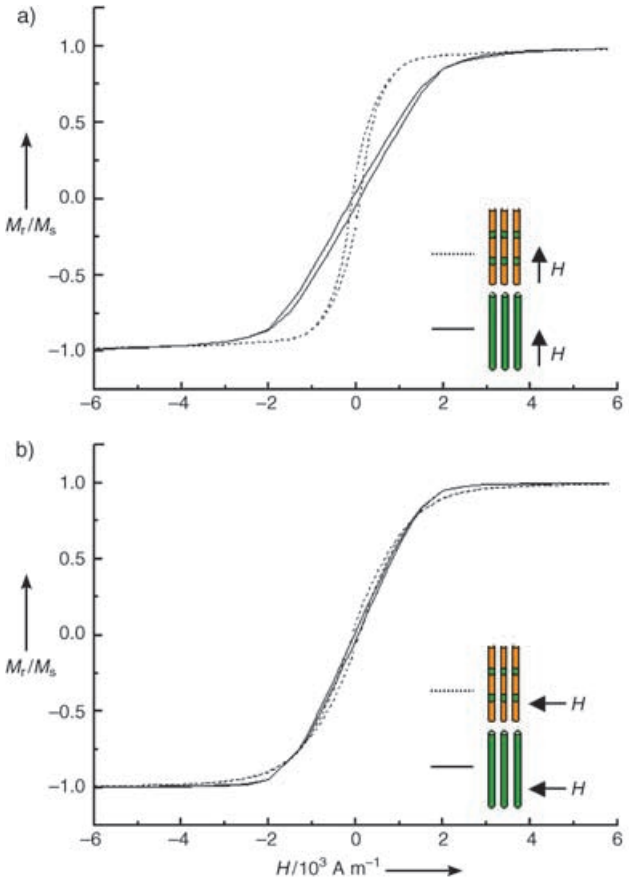

Figure 4. Magnetic hysteresis loops for arrays of Au-Ni-Au-Ni-Au nanotubes shown in Figure 3 (-----) and ferromagnetic Ni nanotubes (——), measured with the applied magnetic field a) parallel and b) perpendicular to the nanotube axis.

multisegmented nanotube arrays could be completely magnetized at lower saturation fields ($H_{s\parallel} \approx 750\ A\,m^{-1}$) than the array of continuous Ni nanotubes ($H_{s\parallel} \approx 2300\ A\,m^{-1}$). The positions of the Ni segments along the pore axis showed large variations (Figure 3a). Although the tube diameter, spacing, and wall thickness for both samples were similar, we assume that the array of multisegmented nanotubes exhibited lower dipolar interactions. The average distance between the neighboring Ni segments was larger than the intertube distance of the continuous nanotube array. In the perpendicular field direction ($\perp$), both samples were completely magnetized around $H_{s\perp} \approx 2000\ A\,m^{-1}$ and show highly similar hysteresis loops with a reversible magnetic behavior ($H_{s\perp} \gg H_{c\perp}$). In comparison of the hysteresis loops for both magnetization directions the array of continuous nanotubes showed a nearly isotropic magnetic behavior, whereas the multisegmented sample exhibited a preferential magnetic orientation along the direction of the magnetic nanotubes as a consequence of the low dipolar interactions and the magnetic anisotropy resulting from the nanotube shape.

In summary, we have developed a simple electrochemical method for the preparation of metal nanotubes. The process is based on the preferential electrodeposition of a metal along the pore walls of an anodic alumina membrane in the presence of Ag nanoparticles on the wall surfaces. We have demonstrated for the first time the preparation of multisegmented metallic nanotubes with a bimetallic stacking configuration along the nanotube axes. This nanofabrication method can be readily extended to a wide range of metallic or semiconducting materials. Furthermore, the unique capacity for tailoring the nanotube structure, along with the functionalization of the inner wall surface of metal nanotubes with various molecules (for example, proteins and DNA), are expected to be particularly useful in the field of catalysis, advanced microfluidics, biological and magnetic sensors, and molecule separation.

Experimental Section

Membrane preparation: Self-ordered nanoporous Al_2O_3 membranes were prepared by the two-step anodization[21] of surface-finished aluminum. In brief, Al sheets (typical diameter 4 cm) were anodized under a regulated cell voltage of 195 V with H_3PO_4 as electrolyte. The first anodization was started under relatively mild electrochemical conditions with H_3PO_4 (0.5 wt.%, 0.6 °C) to prevent the Al from breakdown in the early stages of anodization. After 3 h, the concentration of the H_3PO_4 was increased to 1.0 wt.% by directly injecting 85 wt.% H_3PO_4 into the electrochemical cell, and the temperature of the electrolyte was adjusted to 1.4 °C. The anodization proceeded for 15 h under these conditions. Afterward, the porous oxide layer was completely removed by immersion in an acid mixture (1.8 wt.% chromic acid and 6 wt.% H_3PO_4) at 43 °C for 12 h to obtain a textured surface on the Al sheet. The second anodization was conducted in H_3PO_4 (1.0 wt.%, 1.4 °C) for 16 h. Subsequently, free-standing alumina membranes were obtained by a stepwise voltage reduction technique. The membranes had nominal pore diameters of 300 nm and contained 4.6×10^8 pores per cm^2 of membrane surface area.

Immobilization of metal nanoparticles: The immobilization of metal nanoparticles on the surfaces (pore walls and faces) of an AAO membrane was carried out as follows. First, Sn^{II} was deposited on the surfaces by immersing an AAO membrane in an aqueous mixture of $SnCl_2$ (0.02 M) and HCl (0.01 M) for 2 min. The membrane was thoroughly rinsed in distilled water several times, subsequently in acetone, and finally dried at 70 °C for 1 min. Second, the resulting membrane was dipped into an aqueous solution of $AgNO_3$ (0.02 M) for 2 min to deposit Ag nanoparticles on the pore walls of the AAO, followed by the same drying process used in the first step. These two steps constituted one cycle for metal nanoparticle deposition on the surfaces of a membrane. Typically, six deposition cycles were employed.

Electrodeposition: A thin Au layer was deposited by sputtering on the pore-mouth surface of a nanoparticle-modified AAO membrane to make the surface electrically conductive. This Au layer served as a working electrode in the subsequent electrodeposition of the desired metal. A commercially available plating solution (Auruna 5000) was used for Au nanotubes. Nickel was deposited from a solution of $NiCl_2 \cdot 6H_2O$ (8.41×10^{-2} M), $Ni(H_2NSO_3)_2 \cdot 4H_2O$ (1.59 M), H_3BO_3 (0.33 M), and sodium acetate buffer (pH 3.4). The typical current density was about 2.4 mA cm^{-2}. The total membrane area in contact with the electrolyte was 2.7 cm^2; the total pore area (actual deposition area) was estimated to be 33% of this area.

Received: April 18, 2005
Published online: August 26, 2005

Keywords: electrochemistry · gold · nanotubes · nickel · template synthesis

[1] a) J. Goldberger, R. He, Y. Zhang, S. Lee, H. Yan, H.-J. Choi, P. Yang, *Nature* **2003**, *422*, 599 – 602; b) Z. Liu, D. Zhang, S. Han, C. Li, B. Lei, W. Lu, J. Fang, C. Zhou, *J. Am. Chem. Soc.* **2005**, *127*, 6 – 7; c) Y. J. Xing, Z. H. Xi, Z. Q. Xue, X. D. Zhang, J. H. Song, R. M. Wang, J. Xu, Y. Song, S. L. Zhang, D. P. Yu, *Appl. Phys. Lett.* **2003**, *83*, 1689 – 1691.

[2] a) M. S. Sander, M. J. Côté, W. Gu, B. M. Kile, C. P. Tripp, *Adv. Mater.* **2004**, *16*, 2052 – 2056; b) M. A. Sanchez-Castillo, C. Couto, W. B. Kim, J. A. Dumesic, *Angew. Chem.* **2004**, *116*, 1160 – 1162; *Angew. Chem. Int. Ed.* **2004**, *43*, 1140 – 1142.

[3] a) P. Kohli, M. Wirtz, C. R. Martin, *Electroanalysis* **2004**, *15*, 9 – 18; b) A. Kros, R. J. M. Nolte, N. A. J. M. Sommerdijk, *Adv. Mater.* **2002**, *14*, 1779 – 1782.

[4] a) K. B. Jirage, J. C. Hulteen, C. R. Martin, *Science* **1997**, *278*, 655 – 658; b) S. B. Lee, D. T. Mitchell, L. Trofin, T. K. Nevanen, H. Soderlund, C. R. Martin, *Science* **2002**, *296*, 2198 – 2220; c) S. Yu, S. B. Lee, C. R. Martin, *Anal. Chem.* **2003**, *75*, 1239 – 1244; d) P. Kohli, C. C. Harrell, Z. Cao, R. Gasparac, W. Tan, C. R. Martin, *Science* **2004**, *305*, 984 – 986.

[5] For recent reviews on inorganic nanotubes, see: a) C. N. R. Rao, M. Nath, *Dalton Trans.* **2003**, *1*, 1 – 24; b) M. Remškar, *Adv. Mater.* **2004**, *16*, 1497 – 1504.

[6] a) H. A. Therese, F. Rocker, A. Reiber, J. Li, M. Steputat, G. Glasser, U. Kolb, W. Tremel, *Angew. Chem.* **2005**, *117*, 267 – 270; *Angew. Chem. Int. Ed.* **2005**, *44*, 262 – 265; b) Y. Feldman, E. Wasserman, D. J. Srolovitz, R. Tenne, *Science* **1995**, *267*, 222 – 225.

[7] a) M. Nath, C. N. R. Rao, *Angew. Chem.* **2002**, *114*, 3601 – 3604; *Angew. Chem. Int. Ed.* **2002**, *41*, 3451 – 3454; b) L. Qu, G. Shi, X. Wu, B. Fan, *Adv. Mater.* **2004**, *16*, 1200 – 1203.

[8] a) H. Shin, D.-K. Jeong, J. Lee, M. M. Sung, J. Kim, *Adv. Mater.* **2004**, *16*, 1197 – 1200; b) Y.-S. Min, E. J. Bae, K. S. Jeong, Y. J. Cho, J.-H. Lee, W. B. Choi, G.-S. Park, *Adv. Mater.* **2003**, *15*, 1019 – 1022.

[9] Y. Li, J. Wang, Z. Deng, Y. Wu, X. Sun, D. Yu, P. Yang, *J. Am. Chem. Soc.* **2001**, *123*, 9904 – 9905.

[10] a) Y. Sun, Y. Xia, *Adv. Mater.* **2004**, *16*, 264 – 268; b) B. Mayers, X. C. Jiang, D. Sunderland, B. Cattle, Y. Xia, *J. Am. Chem. Soc.* **2003**, *125*, 13364 – 13365.

[11] a) R. Fan, Y. Wu, D. Li, M. Yue, A. Majumdar, P. Yang, *J. Am. Chem. Soc.* **2003**, *125*, 5254 – 5255; b) T. Kijima, T. Yoshimura, M. Uota, T. Ikeda, D. Fujikawa, S. Mouri, S. Uoyama, *Angew. Chem.* **2004**, *116*, 230 – 234; *Angew. Chem. Int. Ed.* **2004**, *43*, 228 – 232.

[12] a) T. Yanagishita, M. Sasaki, K. Nishio, H. Masuda, *Adv. Mater.* **2004**, *16*, 429 – 432; b) Z. Liang, A. S. Susha, A. Yu, F. Caruso, *Adv. Mater.* **2003**, *15*, 1849 – 1853; c) M. Wirtz, M. Parker, Y. Kobayashi, C. R. Martin, *Chem. Eur. J.* **2002**, *8*, 3573 – 3578; d) G. Wu, L. Zhang, B. Cheng, T. Xie, X. Yuan, *J. Am. Chem. Soc.* **2004**, *126*, 5976 – 5977; e) F.-S. Cai, G.-Y. Zhang, J. Chen, X.-L. Gou, H.-K. Liu, S.-X. Dou, *Angew. Chem.* **2004**, *116*, 4308 – 4312; *Angew. Chem. Int. Ed.* **2004**, *43*, 4212 – 4216; f) P. Kohli, J. E. Wharton, O. Braide, C. R. Martin, *J. Nanosci. Nanotechnol.* **2004**, *4*, 605 – 610; g) J. Bao, C. Tie, Z. Xu, Q. Zhou, D. Shen, Q. Ma, *Adv. Mater.* **2001**, *13*, 1631 – 1633; h) C. Mu, Y. Yu, R. Wang, K. Wu, D. Xu, G. Guo, *Adv. Mater.* **2004**, *16*, 1550 – 1553.

[13] T.-A. Hanaoka, A. Heilmann, M. Kröll, H.-P. Kormann, T. Sawitowski, G. Schmid, P. Jutzi, A. Klipp, U. Kreibig, R. Neuendorf, *Appl. Organomet. Chem.* **1998**, *12*, 367 – 373.

[14] M. Lahav, T. Sehayek, A. Vaskevich, I. Rubinstein, *Angew. Chem.* **2004**, *116*, 5734 – 5737; *Angew. Chem. Int. Ed.* **2003**, *42*, 5576 – 5579.

[15] A. Johansson, J. Lu, J.-O. Carlsson, M. Boman, *J. Appl. Phys.* **2004**, *96*, 5189 – 5194.

[16] a) X. Y. Yuan, G. S. Wu, T. Xie, B. Y. Geng, Y. Lin, G. W. Meng, L. D. Zhang, *Solid State Sci.* **2004**, *6*, 735 – 738; b) X. Y. Yuan, G. S. Wu, T. Xie, Y. Lin, L. D. Zhang, *Nanotechnology* **2004**, *15*, 59 – 61.

[17] a) C. R. Martin, *Science* **1994**, *266*, 1961 – 1966; b) V. P. Menon, C. R. Martin, *Anal. Chem.* **1995**, *67*, 1920 – 1928.

[18] J.-R. Ku, R. Vidu, R. Talroze, P. Stroeve, *J. Am. Chem. Soc.* **2004**, *126*, 15022 – 15023.

[19] S. R. Nicewarner-Peña, R. G. Freeman, B. D. Reiss, L. He, D. J. Peña, I. D. Walton, R. Cromer, C. D. Keating, M. J. Natan, *Science* **2001**, *294*, 137 – 141.

[20] C.-R. Chang, C. M. Lee, J.-S. Yang, *Phys. Rev. B* **1994**, *50*, 6461 – 6464.

[21] a) H. Masuda, K. Yada, A. Osaka, *Jpn. J. Appl. Phys.* **1998**, *37*, L1340 – L1342; b) H. Masuda, M. Satoh, *Jpn. J. Appl. Phys.* **1996**, *35*, L126 – L129.

